Bending and twisting with a pinch: Shape morphing of creased sheets[1].

Steven R. Woodruff[a], Evgueni T. Filipov[a,b,*]

[a] *Department of Civil and Environmental Engineering, University of Michigan, 2350 Hayward St., Ann Arbor, MI 48109, USA*
[b] *Department of Mechanical Engineering, University of Michigan*

Abstract

In this letter, we introduce a unique behavior seen in creased sheets where localized changes in the folding (i.e., a pinch) result in global bending and twisting deformations. Using isometric deformation theory, we identify the connections between pinching, crease curvature, and crease torsion that begin to explain the shape-morphing behavior. Given the limitations of isometric deformations, we expand our understanding of the behavior using a mechanics-based bar and hinge model of creased sheets, where the sheet is allowed to stretch. With this tool, we found that the increase in crease curvature and torsion due to pinching are proportional to the curvature of the crease before folding and that curved creases facilitate the bending and twisting. Additionally, we explored the bending and twisting of sheets with more than one crease. We found that sheets with an odd number of creases generate less intense twisting than those with an even number of creases, even when the creases are straight. The number of creases had little effect on the pinch-induced bending of the origami. The stiffness of the sheets had little effect on the amount of bending and twisting, but greater spacing between the creases resulted in more bending with little effect on the twisting. Based on these results, we created a framework to design crease patterns to have desirable bending and twisting that can be coupled or not, and demonstrated this programmability with simulations and by pinching physical prototypes. Our findings enable shape morphing of creased sheets with a low-complexity input and a versatile output.

Keywords: origami-inspired engineering, curved-crease origami, shape morphing, pinch actuation

1. Introduction

Shape-morphing is the ability to change orientation or geometry in order to alter the intrinsic properties of the system for some functional advantage. Morphing from one configuration to another is achieved using kinematic rotations and translations, mechanical deformations, or a combination of the three. Shape morphing is a foundational property of emerging smart and adaptable structures that use sensors to detect the environment then adapt to that state using actuation. Shape-morphing systems can be found in nature [30, 34] and in a variety of engineering fields, including biomedical engineering [2, 17, 21], aerospace engineering [7, 16], resilient and sustainable infrastructure [4, 11, 14], metamaterials [31, 36], and soft robotics [18, 19, 24, 33].

Implementation of shape-morphing systems in technology faces significant challenges. For instance, shape-morphing often requires expensive materials (e.g., shape-memory alloys or shape-memory polymers) and distributed actuation. Thus, using few and simple actuators is preferred to reduce cost and simplify fabrication [3]. Furthermore, when multiple actuators or distributed actuation are used, controlling the shape of the system becomes increasingly complex. And many existing shape-morphing materials and structures can deform in only one way, limiting the range of shapes the system can attain. Additionally, the parameters determining the final deformed shape can be highly coupled and lead to difficult design frameworks.

Concepts from origami (i.e., folding of thin sheets) and kirigami (i.e., cutting of thin sheets) have inspired novel shape-morphing systems. The advantages of these approaches include simple manufacturing (design and fabrication can start from a flat state), scale independence, and achievable large deformations without permanent damage. Examples of shape-morphing origami and kirigami include adaptable grippers for robotics [40], dynamic façades, locomotive robots inspired by pelican eels [20], and resilient drones inspired by dragonfly wings [27]. However, many origami- and kirigami-inspired systems are limited by the disadvantages experienced by existing

*Corresponding author
Email addresses: stevenrw@umich.edu (Steven R. Woodruff), filipov@umich.edu (Evgueni T. Filipov)

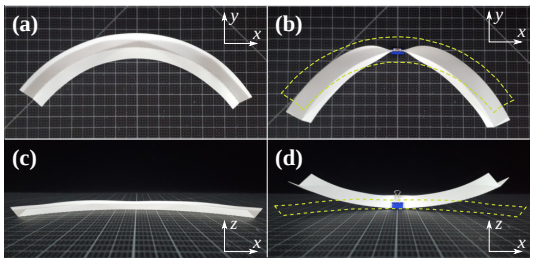

Figure 1: The effects of pinching on a curved-crease polyester sheet. **(a)** A creased annulus sector is folded and has some curvature. **(b)** When pinched at the middle, the structure bends with greater curvature (the unpinched reference shape is shown with dashed lines). **(c)** When unpinched, this creased sheet lies flat on the surface and exhibits no twisting. **(d)** When pinched, the ends of the structure lift, demonstrating a global twisting.

shape-morphing systems explained above (such as requiring multiple actuators), and these structures are also sensitive to imperfections [25].

Beyond the traditional straight-crease origami, curved-crease origami allows folding of thin sheets about arbitrary curves [9]. With curved-crease origami, the sheets between creases always bend upon folding, combining kinematics with deformation mechanics [10]. Designs with curved creases have allowed for unique, tunable stiffness properties [38, 41] and bistable behaviors [6], showing potential for shape morphing using these systems. In this letter, we explore the effect of pinching on curved-crease sheets, where intense folding is applied to a small portion of the crease using a local actuation. Figure 1 shows a creased, circular annulus sector that is folded from polyester sheets (brand name Dura-Lar). When a single pinch is applied at the middle of the structure, it experiences large bending deformation in-plane (i.e., in the xy-plane). Furthermore, we see that the same pinch results in visibly large twisting deformations and a large displacement out-of-plane (in the z-direction).

These curved-crease sheets are capable of significant shape-morphing that include bending and twisting using a single pinch. This deformation is fully reversible, can be prescribed using intuitive crease pattern design, and results in a decoupled, bimodal response with tunable deformation magnitude and sign. In this letter, we introduce the geometric features of curved-crease sheets and isometric theory that form a basis for thinking about how pinching causes deformations (Section 2). With key limitations to isometric theory, we supplement our understanding with a mechanics-based numerical model that allows stretching, and with geometries specifically chosen to help explain the bending and twisting of these structures (Section 3). In Section 4, we investigate the effect that pinching has on the curvature and torsion of a crease that results in global bending and twisting of the structure. We also explore the parameters of origami with more than one crease and how those features affect global twisting and bending. We conclude with a framework for generating tunable bending and twisting, show example crease patterns with desirable behaviors, and present conceptual applications for these shape-morphing systems (Section 5).

2. Theory

2.1. Geometry of curved-crease sheets

In order to understand the relationship between the crease pattern and the effects of pinching, we start by identifying the relevant features of the geometry. An origami structure can be thought of as a set of creases connected by sheets in three dimensions. The crease can be reduced to a parametric space curve in Cartesian coordinates, $\mathbf{c} = \{x(u)\ y(u)\ z(u)\}$, where u is the parameter indicating position along the curve (see Figure 2). In this letter, we consider only curves that are at least three-times continuously differentiable, and we do not consider creases that intersect within the sheet.

The crease, represented as a space curve, will have two important properties that describe its shape. The first is the *curvature* of the crease, κ. Curvature measures the degree to which the crease bends away from its tangent, locally, and can be calculated as,

$$\kappa = \frac{|\mathbf{c}' \times \mathbf{c}''|}{|\mathbf{c}'|^3}, \tag{1}$$

where $(')$ and $('')$ indicate first and second differentiation with respect to, u, respectively, and $(|\ |)$ is the l^2 norm of the vector inside the lines [22].

The second property of the crease we are interested in is its *torsion*, τ. Torsion measures the degree to which the crease turns away from its osculating plane (see **tn**-plane in Figure 2(b)), locally, and can be calculated as,

$$\tau = \frac{(\mathbf{c}' \times \mathbf{c}'') \cdot \mathbf{c}'''}{|\mathbf{c}' \times \mathbf{c}''|^2}. \tag{2}$$

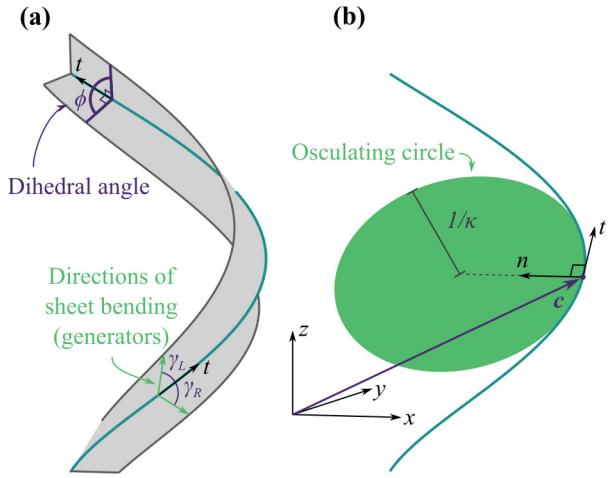

Figure 2: Origami can be represented with surfaces connected to a space curve. **(a)** The deformed shape of creased sheets can be described using the dihedral angle, ϕ, and the generator angles showing the orientation of local sheet bending, γ_L and γ_R. **(b)** With the crease as a space curve, **c**, we can determine the curvature of the crease as the reciprocal of the radius of the osculating circle and the torsion as the rate at which the osculating plane, **tn**-plane (or the normal vector, **n**), twists about the tangent, **t** (defined at each point along the crease).

Here, $(\times)$ indicates the cross product, $(\cdot)$ is the dot product of the vectors, and $(''')$ indicates the third derivative with respect to u [22].

The curvature and torsion describe the local shape of the crease and give insight to the global shape of the structure. We will use these equations to calculate the curvature and torsion of the creases before and after pinching. Because we will use a discrete numerical model (Section 3.1), we estimated the derivatives using a finite-difference calculation that provides a reasonably high-accuracy estimation (errors are of order $O(\Delta u^4)$).

Another important geometric feature of origami structures is the *dihedral angle* of the crease, ϕ. The dihedral angle describes the angle between the sheets extending perpendicular from the crease tangent (see Figure 2(a)), defined at each point along the crease. To prevent the sheets from intersecting upon folding, the dihedral angle is limited to the domain, $0 \leq \phi \leq 2\pi$ [rad]. Figure 3(a) shows examples of the dihedral angle in this domain and Figure 2(a) shows the dihedral angle on a folded sheet. In this paper, all creases with $\phi \in [0, \pi)$ [rad] are mountain creases (indicated with a lighter, blue color) and creases with $\phi \in (\pi, 2\pi]$ [rad] are valley creases (indicated with a darker, purple color). Notice that when $\phi = \pi$ [rad], the sheet is flat.

The first derivative of the dihedral angle with respect to the crease parameter, u, is called the *fold rate*, ϕ'. When the crease is pinched, $\phi' \neq 0$. We use the fold rate to quantify the pinch, and this quantity will be useful in predicting the torsion generated in a crease after pinching.

2.2. *Isometric theory of curved-crease origami*

The properties given in Section 2.1 describe the geometry of the crease at a specific state or configuration. In order to map between different configurations of the crease geometry or deformation states, we can assume that deformations of the origami exist only as bending of the sheets and crease. This is called the *isometric deformation* assumption. Under this assumption, there is no stretching in the sheet or the crease. This is a reasonable assumption given that the in-plane stiffness of the sheet is of order $O(t/l)$, the bending stiffness of the sheet is of order $O([t/l]^3)$, and that $t/l << 1$, where t is the thickness of the sheet and l is the characteristic length [28]. In summary, bending usually requires less energy than stretching, so the system will tend to bend and follow isometric deformations.

From the isometric deformation assumption, we can derive several relationships between the geometry of the crease before folding and after pinching. These equations help us predict the behavior of origami after pinching and set a theoretical basis for why curved-crease origami twist and bend when pinched.

The first relationship we consider describes how the curvature of a crease changes as it is folded. This curvature-folding relation is,

$$\kappa = \frac{\kappa_0}{\sin \phi/2}, \tag{3}$$

where, κ is the curvature of the crease after folding (see Figure 2(b)) and κ_0 is the curvature before folding (when $\phi = \pi$ [rad]) [12, 15, 23]. This equation is plotted as a solid line in Figure 3(a) for a crease with $\kappa_0 = 0.005$ [mm^{-1}].

This relationship shows that as the crease is folded from a flat state, the curvature of the crease will increase as long as $\kappa_0 > 0$ (according to isometric deformation theory).

The second relationship we consider describes the torsion of the crease as it is folded. This relationship can be described with,

$$\tau = \frac{1}{2}\kappa_0 \cot\frac{\phi}{2}\left(\cot\gamma_L + \cot\gamma_R\right), \tag{4}$$

where, γ_L and γ_R are the generator angles on the left and right sides of the crease, respectively (see Figure 2(a)) [23]. The generator angles describe the orientation of bending in the sheets adjacent to the crease and are defined as the angle between the crease tangent, $\mathbf{t}$, and the flat ruling on the surface (i.e., a line segment extending from the crease across the sheet, which exists for all developable surfaces with non-zero mean curvature). The generator angles are limited to the open interval, $(0, \pi)$ [rad]. The direction of bending in the sheet will align with the direction of the generator. Note that when $\gamma_L + \gamma_R = \pi$ [rad], torsion vanishes.

The third relationship is similar to the last, but describes the fold rate of the crease as it is folded. This relationship is,

$$\phi' = -s\kappa_0 \cot\frac{\phi}{2}\left(\cot\gamma_L - \cot\gamma_R\right), \tag{5}$$

where $s = |\mathbf{c}'|$ is the speed of the curve [23]. Again, the fold rate depends on the bending of the sheets adjacent to the crease. Note that when $\gamma_L = \gamma_R$, the fold rate vanishes.

When we combine Equations 4 and 5, we derive a relationship between the crease torsion and the fold rate. Namely,

$$\tau = -\phi'\left(\frac{\cot\gamma_L + \cot\gamma_R}{2s\left[\cot\gamma_L - \cot\gamma_R\right]}\right). \tag{6}$$

We see that torsion can only occur when the fold rate is nonzero. A pinched crease will have a nonzero fold rate; thus, non-zero torsion can occur in pinched structures.

It is difficult to predict what the generator angles will be after folding because the local bending of the sheets depends on the adjacent creases, the forces applied to the sheets, and the restraints on the structure. Because Equation 6 depends on the generator angles, we cannot be certain that pinching will generate torsion or to what degree. Currently, there is no explicit relationship linking the generator angles to the boundary conditions and crease pattern. However, we can implicitly determine the deformed shape of the origami sheets using an energy minimization scheme [5]. Alternatively, we can use a mechanics-based analysis to determine the deformed shape of the origami, as we describe in Section 3.1. Using this method, we can better understand exactly how torsion is related to the curvature of the creases, the dihedral angle, and the fold rate.

For now, we know that crease torsion can only exist when: (1) the flat crease is curved ($\kappa_0 \neq 0$), (2) the crease is folded away from a flat state ($\phi \neq \pi$ [rad]), and (3) the crease is allowed to diverge from its originally flat plane (there can be no boundary conditions preventing twisting). Curvature will always exist for an initially curved crease.

2.3. Limitations of isometric theory

From Equation 3, isometric deformation theory tells us that as a curved crease approaches complete folding ($\phi \to 0$ or $\phi \to 2\pi$ [rad]), the curvature of that crease will approach infinity. Intuitively, this seems incorrect. Indeed, when a paper prototype of a curved-crease origami is folded completely, the sheets appears to flatten out, rather than curve infinitely. This flattening suggests that the isometric deformation assumption fails to describe the deformed shape of real origami structures, where stretching is possible, at least for some domain of dihedral angles. And pinching does result in near-complete folding of a crease. Thus, if we are to examine how pinching affects the shape of origami structures, we need to understand the limitations of the isometric deformation assumption and suggest a more versatile means of determining the deformations of curved-crease origami.

An alternative to isometric theory is to perform a mechanics-based analysis on an origami structure. We use a numerical model to simulate the folding and pinching of origami, which is described in Section 3.1. This numerical model calculates the equilibrium state of the origami structure in response to forces and/or moments that generate folding. The model includes bending, folding, and stretching deformations, allowing for possible in-plane deformations ignored in isometric theory. The numerical model uses elastic elements with a nonlinear geometric response. We use this numerical model to explore the performance of the isometric deformations assumption under different degrees of folding.

Figure 3(a) shows the normalized curvature, κ/κ_0, of a crease with $\kappa_0 = 0.005$ [mm^{-1}] after folding with the corresponding dihedral angle, ϕ. The origami used in Figure 3 is a circular annulus sector that is creased along its mid-radius to a dihedral angle, ϕ, which is held constant along the crease length (see Figure 3(d)(i)). We see that the curvature ratio aligns with the isometric theory for moderately folded dihedral angles ($\pi/3 \leq \phi \leq 5\pi/3$ [rad]). However, for more complete folds, the numerical model starts to diverge from the isometric theory.

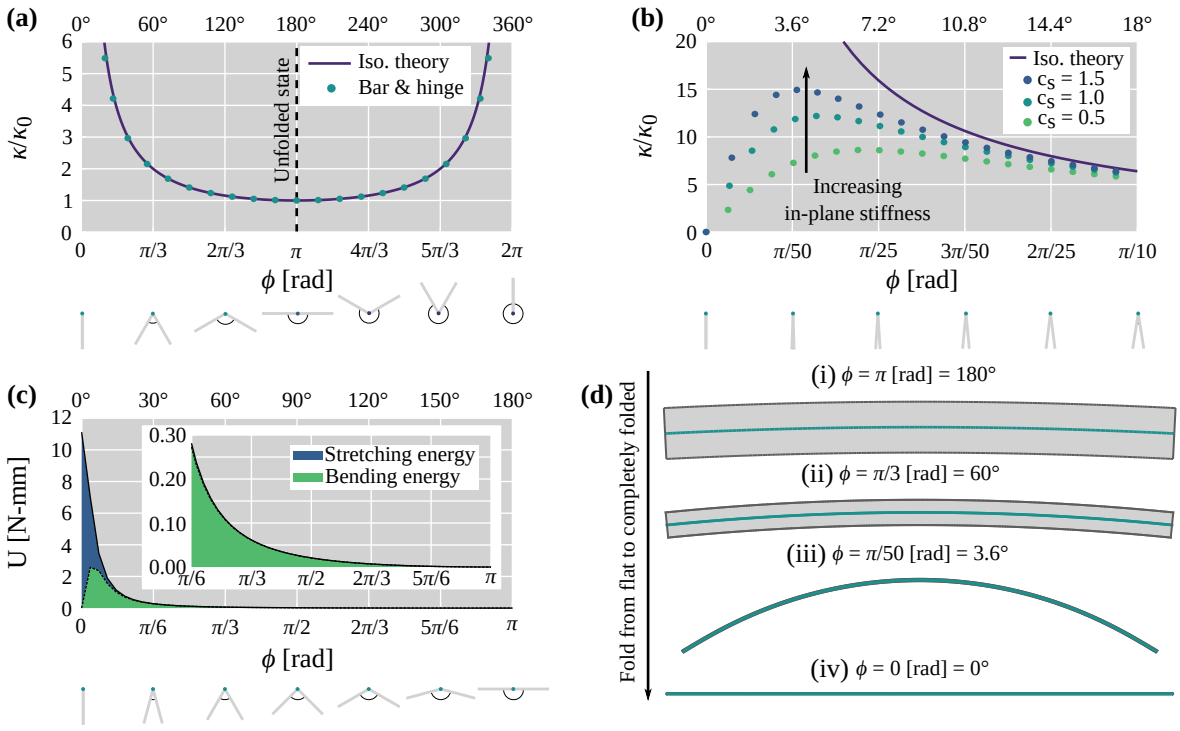

Figure 3: Isometric deformation of thin sheets is a valid assumption for a limited range of folding, but is insufficient for pinching folds. **(a)** The curvature of a curved-crease annulus before, $\kappa_0 = 0.005$ [mm^{-1}], and after, κ, folding is the same for the isometric theory and a bar and hinge model in a large domain of dihedral angles (the images below the x-axis show the cross-section of the origami and the corresponding dihedral angle of the annulus sector at some point along its length, with the tangent vector pointing into the page). **(b)** For dihedral angles approaching complete folding, the curvature peaks and falls to zero with the numerical model, rather than approaching infinity. The stiffness of the sheet in stretching (multiplied by a factor, c_s) impacts the change in curvature, suggesting that in-plane deformations dominate at extreme dihedral angles. **(c)** The strain energy in the bar and hinge model shows that the stretching energy dominates for extreme dihedral angles, defying the assumption that deformations are predominantly in bending. **(d)** The folded shape of origami shows crease curvature increases as it is folded, peaks, then flattens to avoid infinite curvature once the dihedral angle is zero.

Figure 3(b) shows the normalized curvature, but for dihedral angles close to complete folding ($0 \leq \phi \leq \pi/10$ [rad]). We see that as the dihedral angle approaches zero, the curvature of the numerical model is significantly less than what isometric theory predicts. After $\pi/50$ [rad], the curvature of the model starts to decrease, and the crease flattens when completely folded (see Figure 3(d)). We changed the stretching stiffness in the mechanics-based model by a factor of c_s to see how the crease curvatures changed, and saw that the stiffer models ($c_s = 1.5$) would curve more than the models with less stiffness ($c_s = 0.5$), but all mechanics-based models eventually flattened to zero curvature.

When we determine the shape of origami after folding using a mechanics-based model and allow the sheets to stretch, we find that approaching complete folding of curved-crease origami results in flattening, rather than infinite curvature. Because the origami flattens as it is completely folded, and the normalized curvature is related to the stretching stiffness of the model, this indicates that stretching is important for the sheets in highly folded configurations. Indeed, Figure 3(c) shows that as the dihedral angle approaches zero, the bending strain energy decreases and stretching strain energy increases. Effectively, stretching and flattening the sheet becomes more energetically efficient than it is to bend the sheet to an infinite curvature. This result holds for the other folding extreme as $\phi \rightarrow 2\pi$ [rad]. Using a finite-element model with identical material properties and dihedral angles, we found that in-plane deformations also occur in the sheet and are located near the crease, supporting our claim that isogeometric theory fails to capture the deformation of origami made from elastic sheets at extreme dihedral angles, where stretching occurs.

From these results, we know that isometric deformations are a reasonable assumption for moderately folded origami ($\pi/3 \leq \phi \leq 5\pi/3$ [rad]), but we should expect stretching deformations to occur for dihedral angles outside of this domain; specifically, at a region near where a crease is pinched. We can use the isometric relationships to gain insight on how real origami structures work, especially for folding, but we need to use a more versatile method to explore the effects pinching has on a structure.

3. Materials and methods

3.1. Bar and hinge modeling of creased sheets

In order to supplement the isometric theory for exploring how pinching affects the deformed shape of creased sheets, we used a numerical model to simulate the folding and pinching of thin sheets. This method, called *the bar and hinge model* [13, 26, 32], represents sheet deformations using three elements. The first is a three-dimensional truss element called a bar, which combined with other bars captures the in-plane deformations of the sheet (i.e., stretching and shearing). The second element is a hinge, or a rotational spring, that captures bending deformations of the sheet by lumping the bending into discrete rotations. The third element is also a hinge, but captures crease rotations due to folding.

The combination of these three elements allows us to model the deformation of origami structures under folding and post-fold loading (e.g., a pinch). Each element is assigned a stiffness value, which has been calibrated to the physical stiffness of thin sheets based on the mesh size, thickness of the sheet, and the sheet material properties [37]. The bar and hinge model arrives at a solution using a Newton-Raphson solver, accommodating geometric non-linearity [39]. The bar and hinge model can capture the deformation of curved-crease origami with a reasonably high accuracy. Indeed, comparing the deformed shape of several hand-folded paper sheets to simulated bar and hinge models gave an average Hausdorff distance error of 0.4% the maximum length of the models [37]. And, because the bar and hinge model uses fewer elements than a finite elements model, convergence occurs in less time (in the geometries depicted in this paper, usually less than ten seconds) and with a greater rate of successful convergence.

We use the bar and hinge model to capture the deformed shape of the folded and pinched sheets described below. The data we collect from the models are used to calculate the torsion and curvature of the creases and the global twisting and bending of the structure.

3.2. Model geometries and parameters

All of the curved-crease sheets studied in this work shared certain geometric features and parameters. First, all of the creases and edges were uniformly spaced, meaning the distance between each crease and between the creases and the edges were some set distance, w. Using uniform crease spacing eliminates twisting due to folding, a source of twisting distinct from the pinch-induced twisting investigated here, because uniformly spaced creases fold to a mostly torsion-free configuration (small amounts of torsion will occur near the ends of the creases, but this torsion is minor [5]). Next, all models were restrained so that the sheets were free to fold without generating noticeable twisting and could be freely pinched while maintaining global stability. All restraints lie on the line extending from the pinch force in the flat plane (at the midpoint along each crease). Finally, every model was designed from a flat crease pattern, ensuring developability so the origami could be easily fabricated.

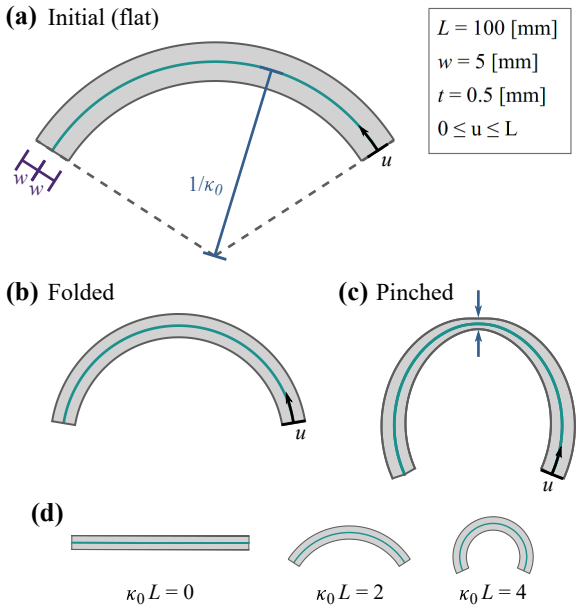

Figure 4: Single-crease, annulus sectors share common geometric properties. **(a)** The structure starts as a flat crease pattern with a constant initial curvature, κ_0. **(b)** As the structure is folded, the curvature increases. **(c)** After folding, the sheet is then pinched at the mid-length and the curvature and torsion are calculated. **(d)** Annulus sectors with different initial curvatures.

The first set of model simulations explored the curvature and torsion that occurs from pinching on a single-crease sheet structure. For these analyses, the crease pattern is a circular annulus sector creased at mid-radius (see Figure 4). Each of the creases had a constant length, $L = 100$ [mm], were folded to $\phi_R = \pi/2$ [rad] (90°), were spaced $w = 5$ [mm] from the edges, and the stiffness factor of the creases was $L^* = 2$ [mm] [13]. The sheets had constant thickness, $t = 0.5$ [mm] and elastic modulus, $E = 4000$ [N-mm]. The creases were pinched to the dihedral angles shown in Figure 5(a), with a minimum dihedral angle, ϕ_p, of $\pi/14$ [rad] (12.86°). This minimum dihedral angle was chosen to ensure model convergence and to avoid local instabilities, such as sheet wrinkling, which are sometimes seen in models with high initial crease curvature. The curvature of the creases before folding, κ_0, varied from zero to 0.05 [mm^{-1}] (see example unfolded shapes in Figure 4(d)).

For the second set of analyses, we used models with multiple creases to see the effects of other factors that become important with more than one crease (i.e., number of creases, sheet stiffness, and crease spacing). For these simulations, the geometry was again a creased annulus sector where the crease with the lowest curvature was a mountain crease, had a length, $L = 100$ [mm], and all references to crease curvature are the curvature of that crease. The creases alternate between mountain and valley folds where the mountain creases were folded to $\phi_m = \pi/2$ [rad] (90°), and the valley creases were folded to $\phi_v = 3\pi/2$ [rad] (270°). The creases were pinched so that the dihedral angles were $\pi/18$ [rad] (10°) away from being completely folded. The stiffness factor of the creases was $L^* = 2$ [mm]. The thickness of the sheets was, $t = 0.5$ [mm], except for the analyses varying sheet stiffness. The spacing between the creases and the edges was $w = 5$ [mm], except for the simulations varying crease spacing, and the number of creases was three, except for the analyses varying this value. Each of the analyses were run with three different initial crease curvatures ($\kappa_0 = 0,\ 0.005,\ 0.01$ [mm^{-1}]).

4. Results

4.1. Local effects of pinching

Curvature and torsion describe the manner in which a curve is moving through space, relative to nearby points on the curve. The curvature tells us how the curve is bending and torsion tells us how the curve is twisting, both on a local scale. Curvature and torsion do not directly explain the total amount of bending and twisting. But, in general, greater curvature and greater torsion will lead to more bending and twisting, respectively. As an analogy, curvature and torsion are to bending and twisting as strains are to deformations. Understanding the local curvature and torsion generated from pinching will help link the crease pattern parameters to global deformations.

Figure 6(a) shows the curvature along the length (i.e., the curvature profile) of an annulus sector creased at mid-radius and pinched at mid-length. The curvature profile was found for crease patterns with varying initial curvatures. We see that for all crease patterns with non-zero initial curvature, the curvature of the crease increases

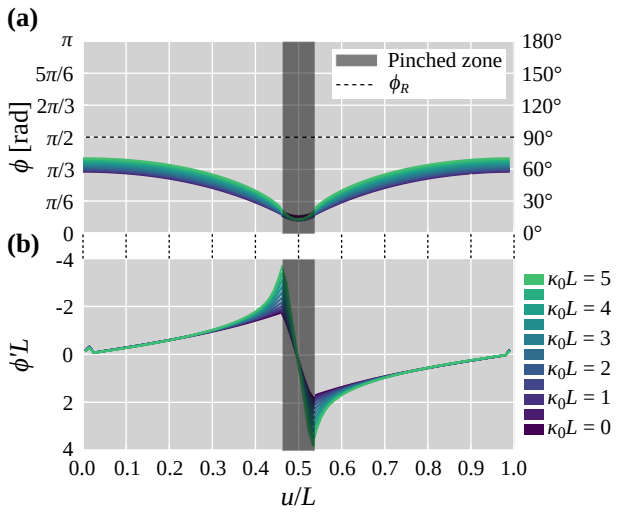

Figure 5: Pinching varies the dihedral angle, ϕ, and fold rate, ϕ', of the creased sheet for various initial curvatures, κ_0. **(a)** The dihedral angle of a pinched mountain crease decreases near the pinch into the domain where isometric theory fails. **(b)** The fold rate for a pinched crease is non-zero, especially near the pinch.

drastically just outside the pinch location then tapers down towards the curvature we expect from the folded, non-pinched shape. Within the pinched zone (i.e., the portion of the crease length where pinching forces were applied), the curvature is significantly reduced. This reduction occurs because the high degree of folding does not allow isometric deformations. The pinching causes local flattening and a reduction in curvature (as shown in Figure 3). We see that pinching generates a local, highly curved portion of the structure that acts as a hinge and generates global bending. Note that towards the ends of the crease ($u/L \approx 0$ and $u/L \approx 1$), there are errors in the curvature calculation that stem from the finite difference approximations of the derivatives. These errors do not affect the results away from the ends.

For each initial curvature, the peak value, κ_p, was measured, with the location of this peak near the edge of the pinched zone (indicated in Figure 6(a) with a dotted line). This peak curvature was plotted against the initial curvature in Figure 6(b). We see that the peak curvature is proportional to the initial curvature of the crease, indicating that greater local curvature from a pinch can be gained with higher initial curvatures.

Figure 7(a) shows the torsion along the length (i.e., the torsion profile) of the same circular creased annuli. We see that pinching results in large crease torsion for creases with nonzero initial curvature. The torsion in the crease peaks near the pinch, then tapers down to zero moving away from the pinch. Notice that the shape of the torsion profile is similar to that of the fold-rate profile shown in Figure 5(b) (the vertical axes on this plot are reversed to accommodate the negative relation between torsion and fold rate given in Equation 6). This similarity between the fold-rate profile and the torsion profile suggest that the rate of change of the dihedral angle could be useful for prescribing a desired torsion profile. Additionally, the magnitude of torsion appears to increase with the initial curvature of the crease, suggesting that the shape of the torsion profile can also be scaled by altering the initial curvature of the pinched creases. Again, the torsion values near the ends of the crease are erroneous due to approximation errors and should not be considered an accurate reflection of the crease torsion.

Figure 7(b) shows how the peak torsion, τ_p, varies with the initial curvature of the crease. The peak torsion was measured along the dotted, black line in Figure 7(a), just outside the pinch where the torsion profiles peak. We see that the peak torsion is proportional to the initial curvature of the crease. This confirms that the amount of twisting in the structure can be prescribed by varying the initial curvature of the crease.

In these analyses, the creases were all folded to mountain folds, but the curvature and torsion of valley folds will be the same (because curvature and torsion are intrinsic properties of the curve and do not vary with the coordinate system). The global bending and twisting do depend on the mountain/valley crease assignment, but are related to each other. We see from the inset deformed shapes in Figure 6(b) that pinching the sheets increases the curvature of the crease, resulting in bending towards the center of curvature. Bending towards the center of curvature will occur for both mountain and valley creases. For twisting, we see in Figure 7(b) that the torsion of the crease causes the structures to twist downward due to the pinch (for the case where the mountain crease lies on top of the sheets). For a valley crease, the origami would twist upward. Formally, pinching a curved crease will result in the sheet to move opposite the direction of the binormal vector, or the vector describing the positive normal to the osculating plane (see the **tn**-plane in Figure 2(b)). In more relatable terms, the origami will twist away from the direction the crease is pointing, where in this case, mountain creases point upward and valley creases point

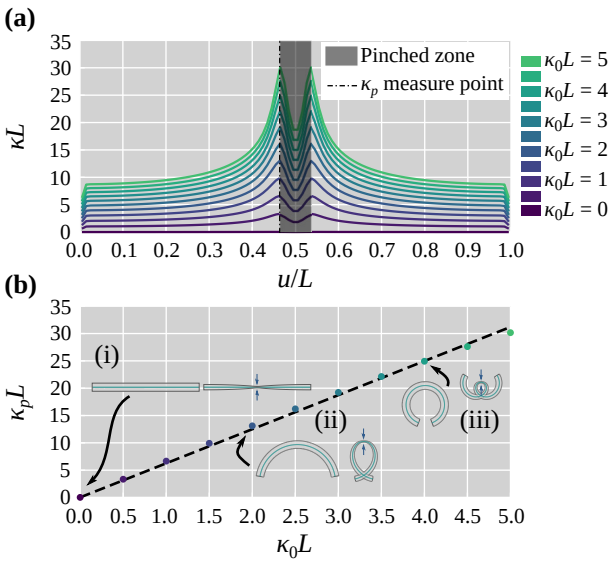

Figure 6: **(a)** Pinching single-crease sheets causes changes in the curvature of the crease along its length, u. For all geometries where the initial curvature, κ_0, is not zero, the resulting curvature, κ, will increase near the pinch point and taper off towards the ends. **(b)** The peak curvature upon pinching, κ_p, is proportional to the initial curvature of the crease pattern (inset images (i-iii) show the folded [left] and pinched [right] shapes, displaying the increase in curvature).

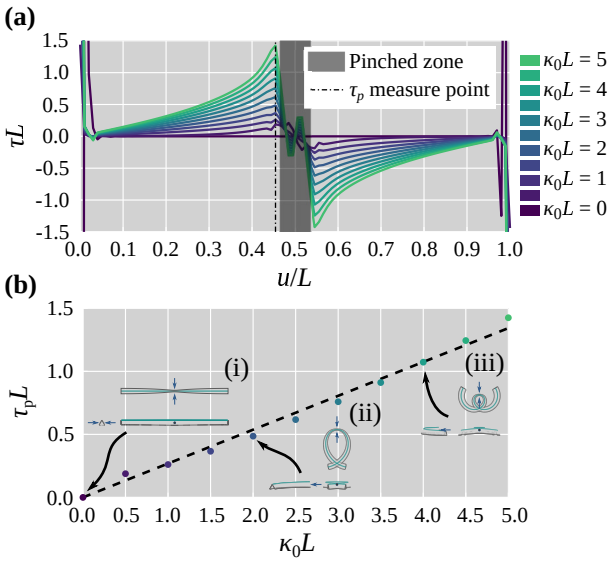

Figure 7: Pinching single-crease sheets with non-zero initial curvature causes a large increase in the torsion, τ, of the crease. **(a)** Upon pinching, the crease torsion increases near the pinch then tapers off. **(b)** The peak torsion, τ_p, is proportional to the initial curvature, κ_0, of the crease pattern (inset images (i-iii) show the top, front, and side views of various origami models, showing twisting deflections).

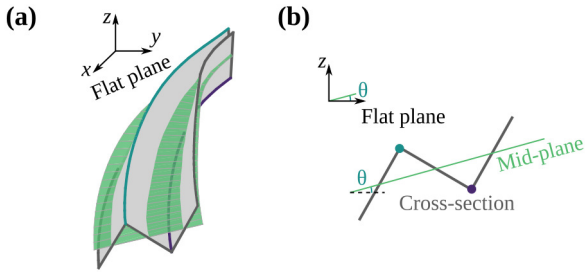

Figure 8: Unlike torsion, the global twisting of a multi-crease system depends on the coordinate system. **(a)** At each point along the length of the crease, a mid-plane is calculated, splitting the origami into an upper and lower portion. **(b)** The mid-plane with respect to the cross-section. The twist angle, θ, is calculated from the xy-plane, and the twist angle at the ends are used to measure global twisting.

downward.

4.2. Deformations of pinched sheets with multiple creases

When sheets are folded with more than one crease, the deformations of the creases become coupled, and properties of the sheet become important to the global behavior [8, 35]. These parameters of interest include the number of creases in the crease pattern, the stiffness of the sheet determined from its thickness and elastic modulus, and the spacing between the creases. We varied the aforementioned parameters and found the deformed shape of pinched origami with multiple creases and measured the effect on global bending and twisting of the structures.

To measure bending and twisting of multi-crease origami, we start by finding the mid-plane that cuts the cross-section through the middle (see Figure 8). The mid-plane is calculated at each point along the length of the origami by forming a line between the point that lies between the edge and the first crease and the point between the last crease and the adjacent edge. These lines are connected to form a surface representing the mid-plane. The bending angle for the multi-crease origami is the angle between the lines extending from the center of the mid-length of the mid-plane (the location of the pinch) to the center of the mid-plane at the ends of the structure. To measure the bending behavior due to pinching, the bending angle was calculated after folding the origami, β_f, and after pinching, β, and the difference between the two was calculated (see Figure 11(c)). The change in twisting angle, $\theta_f - \theta$, was measured as the angle between the mid-plane at the right end of the structures and the flat plane (xy-plane, where the unfolded origami lies) for the folded (θ_f) and pinched (θ) configurations.

Figure 9(a) shows the change in bending angle from pinching the origami with different number of creases for three different initial curvatures. The reported initial curvature is for the topmost crease, which has the lowest curvature of all creases in the sheet. We see that the number of creases is not strongly related to the amount of bending. Because all the creases share a center of curvature, all creases bend towards that direction without disruption from adjacent creases.

Figure 9(b) shows that the number of creases has a large effect on the twisting of the structure. The first trend we see is the difference between origami with an even number of creases and those with an odd number of creases. Origami with an odd number of creases will exhibit a smaller, positive twisting angle, while origami with an even number of creases will twist in the negative direction significantly more. The different twisting for even and odd creases holds for the origami with zero initial curvature, but, the torsion for odd-numbered creases is always zero. Figures 9(c-d) show cross-sections of the two- and three-crease geometries at the pinch and at the right end of the structure, along with photographs of prototypes with the same crease patterns. All physical prototypes presented in this paper are made from polyester sheets supplied by Dura-Lar and have a thickness of 0.127 [mm]. For both the two- and three-crease models, the outermost sheets barely rotate away from the pinch. Because for the two-crease model, the sheets are parallel, pinching causes the mid-sheet to rotate away from the pinch, causing the global twisting. For the three-crease model, the outermost sheets are mirrored, and the center sheets do not rotate away from the pinch. The different twisting behavior for an even versus odd number of creases holds for origami with a greater number of creases and for those with non-zero curvature as well.

Another trend that we see when varying the number of creases requires separating the even- and odd-crease origami and looking at each individually. Looking at the twist angles separately, we see that as more creases are added, the magnitude of twisting decreases, suggesting that origami with a high number of creases (e.g., seven) will show little twisting, especially if there are an odd number of creases.

Figure 10(a) shows the change in bending angle for a three-crease model when the stiffness of the sheet is varied. We see that the sheet stiffness has a small effect on the amount of bending in the origami. The effect is most pronounced for sheets with low stiffness ($Et^3 < 2000$ [N-mm]) and higher curvature. However, the overall effect is small with only an increase of 9.80% for halving the stiffness from 1000 [N-mm] to 500 [N-mm] (for

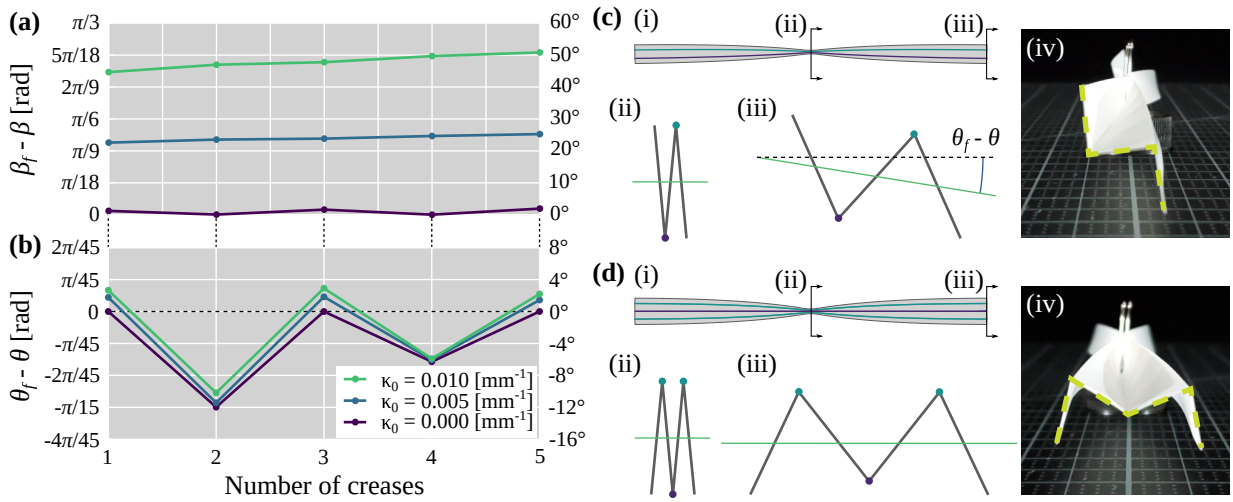

Figure 9: Effect of crease number on bending and twisting. **(a)** The change in bending angle due to pinching, $\beta_f - \beta$, does not vary substantially with the number of creases for all initial crease curvatures, κ_0. **(b)** The change in twist angle, $\theta_f - \theta$, is greatly affected by the number creases. **(c)**(i) An origami structure with two creases and $\kappa_0 = 0$ is folded and pinched. (ii) The cross-section at the mid-length has no twisting, but (iii) the cross-section at the end is twisted. (iv) A photograph of the same model made with Dura-Lar shows the same behavior (dashed lines added for emphasis). **(d)** For an origami structure with three creases, there is no twisting.

$\kappa_0 = 0.01$ [mm^{-1}]). A similar trend can be seen with twisting in Figure 10(b) with only an increase of 9.93% in twisting angle change when reducing stiffness from 1000 [N-mm] to 500 [N-mm] (for $\kappa_0 = 0.01$ [mm^{-1}]).

The flexibility of the sheet will determine its compliance to the crease shapes (i.e., a more flexible sheet will reconfigure to comply with the curvature and torsion of a crease than a stiffer sheet). However, the influence of stiffness is small, and the bending and twisting are affected more by the shape of the origami (e.g., κ_0).

The last multi-crease parameter we explored was crease spacing. Figure 11(a) shows the change in bending angle versus the distance between the creases. We see here that bending is proportional to crease spacing. The greater creases are spaced, the more bending we see. For twisting, greater crease spacing results in more twisting, but the effect is non-linear and is less than with bending (see Figure 11(b)).

It is important to note that as the crease spacing increases, stretching (due to the extreme folding described in Section 2.3) increases at the edges away from the creases. This stretching can result in local instabilities of the sheet (e.g, wrinkling), seen in both the bar and hinge model and in physical, polyester prototypes. As such, there is a practical limit to the crease spacing that depends on the material properties of the sheet.

5. Discussion

From the single and multi-crease analyses, we have a better understanding of the crease pattern and sheet properties that cause bending and twisting of uniformly spaced origami when pinched. We can use this understanding to establish a framework for prescribing pinch-induced deformations to origami to meet the needs of an adaptable system. We will then use this framework to create example crease patterns that display various combinations of deformations.

5.1. Generating and tuning global bending

When origami is pinched, the curvature of the creases (for crease with non-zero initial curvature) increases near the pinch. This increase in curvature generates a hinge that rotates the ends of the structure, causing the origami to bend globally. The greater the initial curvature of the crease, the more it will bend upon pinching. When a curved-crease origami is pinched, the bending is towards the center of curvature. Because the center of curvature is the same for mountain and valley creases, pinching either type of crease will result in the same bending deformation, even with multiple creases. The number of creases in a multi-crease pattern does not influence the magnitude of bending, and a more flexible sheet will bend slightly more than a stiffer sheet, but stiffness has a minimal effect on bending. Finally, multi-crease systems with a greater crease spacing will generate greater bending (until local instabilities occur for large crease spacing).

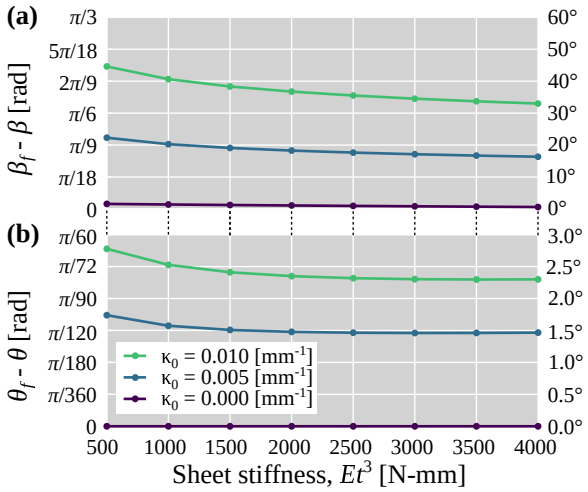

Figure 10: Effect of sheet stiffness on bending and twisting. **(a)** The change in bending angle, $\beta_f - \beta$, and **(b)** the change in twisting angle, $\theta_f - \theta$, due to pinching are slightly greater for more flexible sheets.

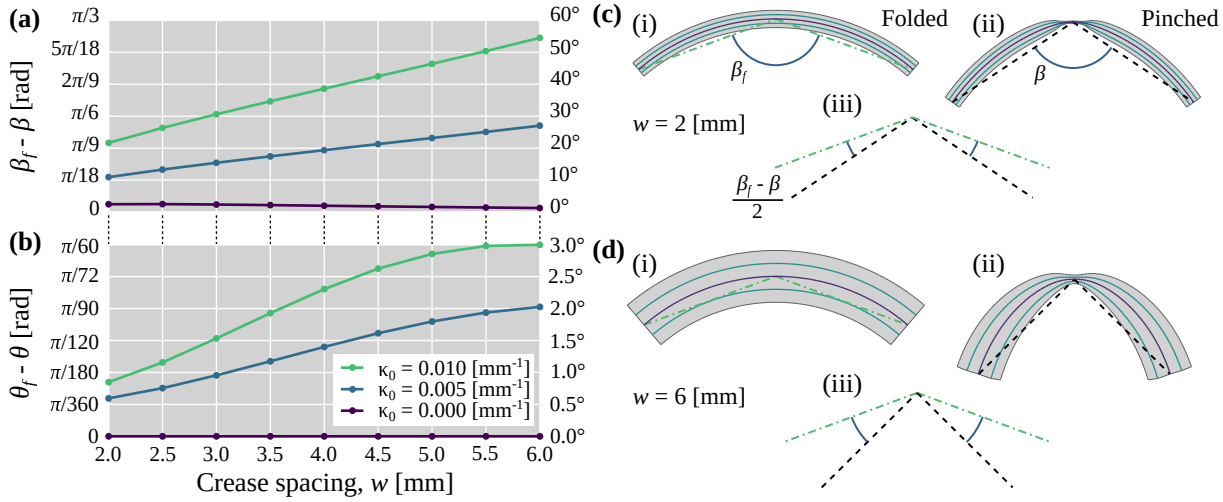

Figure 11: Effect of crease spacing on bending and twisting. **(a)** The change in bending angle due to pinching, $\beta_f - \beta$, is proportional to the crease spacing with substantial effect for all non-zero initial curvatures, κ_0. **(b)** Larger crease spacing also increases twisting, but has a non-linear effect. **(c)** A three-crease model with w = 2 [mm] is (i) folded and (ii) pinched, with the change in bend angle shown separately in (iii). **(d)** For a three-crease model with w = 6 [mm], the bend angle change is more substantial.

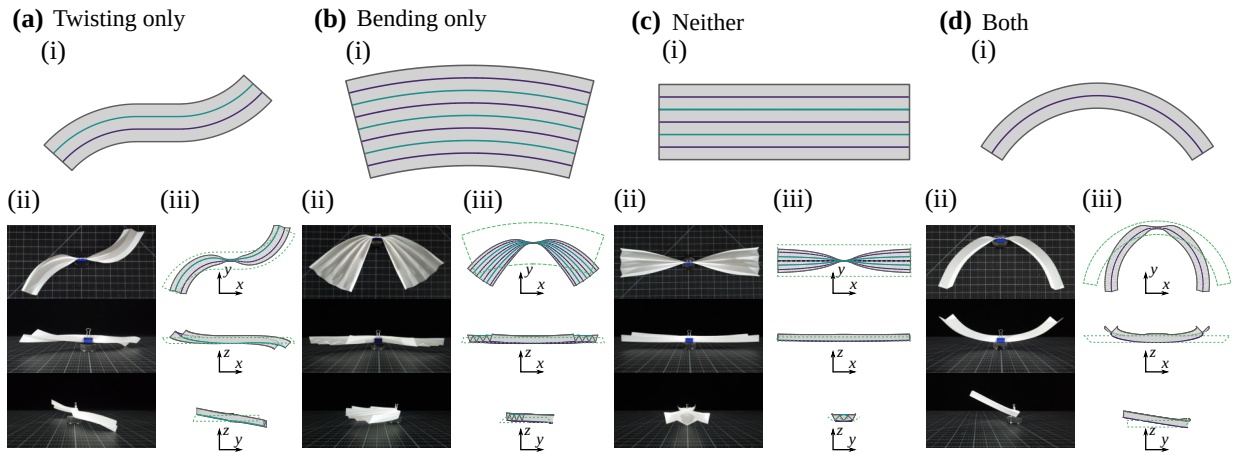

Figure 12: The framework described in Section 5 is used to design four crease patterns with desired pinch-driven twisting and bending deformations. **(a-d)**(i) The initial crease patterns. (ii) The pinched shape of physical models made from polyester sheets are similar to (iii) the deformed shapes found using the bar and hinge method and validate the framework (dotted lines show the folded and unpinched configuration).

5.2. Generating and tuning global twisting

When curved creases are pinched, large torsion deformations appear near the pinch. The torsion peaks near the pinch, then tapers off towards zero away from the actuation. This torsion, along with other factors, result in global twisting in the structure. For origami with an odd number of creases, greater crease curvature will generate greater twisting. Origami with an even number of creases will generate large amounts of twisting, but this larger twisting is caused predominantly by the sheet arrangement, not the crease curvature. Mountain and valley creases will generate torsion of an opposite sign, so a single mountain crease that is pinched will deflect in one direction (the direction opposite the that of the crease's binormal vector), and a valley crease of the same shape will deflect in the other (where the binormal vector is flipped). Like bending, more flexible sheets twist slightly more than a stiffer sheet. Again, the sheet stiffness has a minimal effect. Wider crease spacing will also generate greater twisting, due to the lever arm that the sheets make between the creases.

5.3. Crease patterns for isolated or combined bending and twisting

With this framework, we can create crease patterns that display desired bending and twisting behaviors. Figure 12(a)(i) shows a crease pattern that, when pinched, experiences large twisting, but minimal bending deformations. The crease pattern has zero curvature near the center (where the pinch occurs) and has non-zero curvature near the ends. This crease pattern also uses two creases, which will generate large twisting along the curved ends of the origami. Figures 12(a)(ii-iii) show the effect of folding and pinching on this geometry, where there is no global bending, but large twisting at the ends.

The second geometry we created displays only bending deformations when pinched. Figure 12(b)(i) shows a crease pattern that has non-zero initial curvature everywhere, but has a large and odd number of creases (seven). Figures 12(b)(ii-iii) show that pinching the structure results in significant bending with minimal twisting deformation.

Figure 12(c) shows the third geometry that displays neither bending nor twisting when pinched. The crease pattern has zero initial curvature and an odd number of creases (five). Pinching this structure gives a neutral local deformation in the middle, with no global deformations (see Figures 12(c)(ii-iii)).

The fourth and final geometry displays both bending and twisting due to pinching. Figure 12(d)(i) shows a single-crease, annulus sector crease pattern with a non-zero curvature. Pinching this structure generates significant bending and twisting deformations, as shown in Figures 12(d)(ii-iii).

These four geometries show only a small subset of possible crease patterns that will display isolated and combined bending and twisting behaviors. By varying the initial crease curvatures, number of creases, and crease spacing, the magnitude of these deformations can also be controlled, as needed.

Pinched shape-morphing origami have the potential to advance technology in a variety of fields, with applications requiring targeted changes in the shape of the mechanism with little actuation complexity. Pinching can occur at any point along the length of a crease and with multiple pinches for applications in soft robotics, such as a gripper (see Figure 13(a)). Additionally, a dynamic façade [1, 29] composed of curved-crease panels can twist away from a building and bend to allow light in, as needed (see Figure 13(b)). Another potential application of shape-morphing origami is adaptable, architected materials that require simple actuation, but high complexity

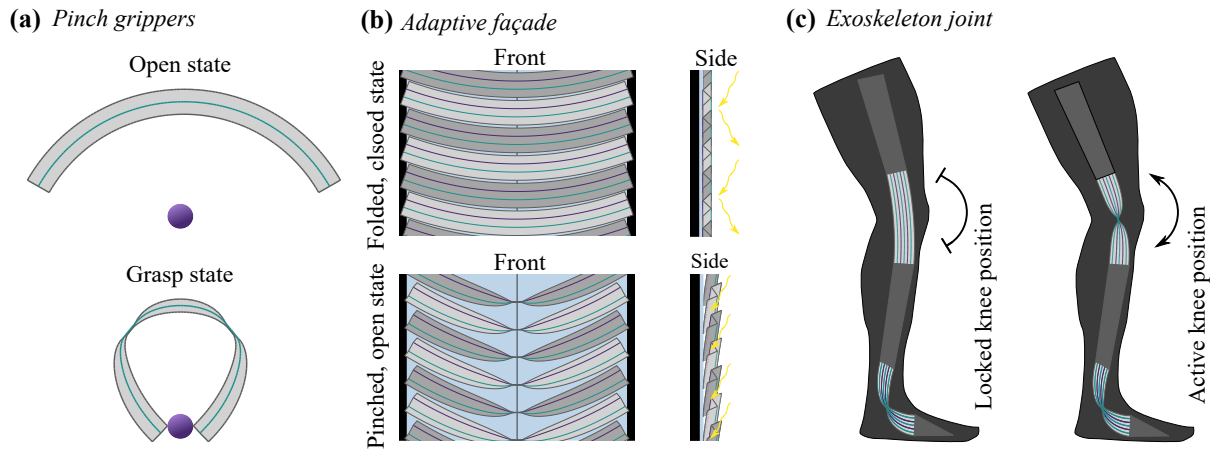

Figure 13: Conceptual applications of pinch-actuated origami. **(a)** Pinches can be applied to curved-crease origami to generate intense bending along the length of the crease to achieve grasping-type motions. **(b)** An origami façade can be adapted to optimize the heat and light entering a building depending on internal and external conditions. Both bending and twisting motions can be achieved with a simple pinch. **(c)** A curved-crease sheet with an odd number of creases (limited twisting upon pinching) could allow for an exoskeleton-type system that locks or allows bending, as needed.

shape changes. Finally, our findings could support development of exoskeletons that can morph to the shape and functional needs of the wearer in real-time and generate a hinge with a locked, high-stiffness state and an unlocked, low-stiffness state using pinching (see Figure 13(c)). The adaptive stiffness for this type of pinched mechanism was demonstrated in our previous work [37].

6. Conclusion

When creased sheets are pinched, the deformed shapes can bend and twist in desirable ways to achieve a new, geometric state. Using pinching for shape morphing of creased sheets overcomes many of the obstacles facing existing adaptable materials and structures. For instance, the inputs to the system are a single-degree-of-freedom actuation that results in variable intensity bending and twisting that can be coupled or isolated and is fully reversible. By limiting the number and distribution of actuation points, the shape-morphing system becomes less complex and less expensive, requiring fewer actuation elements made from costly materials (e.g., shape-morphing alloys/polymers or piezoelectric actuators). The control system for shape-morphing origami is relatively straightforward, with the crease design and pinch location determining the magnitude and sign of global bending and twisting.

Isometric deformation theory predicts the increase in curvature and torsion caused by pinching, but it limited to moderate dihedral angles ($\pi/3 \leq \phi \leq 5\pi/3$ [rad]) and requires understanding how sheet bending is linked to the boundary conditions of the structure. Our results using a mechanics-based numerical models confirm that origami with creases of higher initial curvature will generate greater curvature and torsion in the area surrounding the pinch. However, the increase in curvature exists only outside the pinched zone, and the sheet will flatten at the pinch (a result that isometric theory does not explain). These local behaviors affect the global deformation of the structure. When a sheet is folded about more than one crease, the number of creases does not influence the amount of bending seen in origami, but significantly affects the magnitude and sign of twisting. Origami with an even number of creases will result in large, negative twisting, and origami with an odd number of creases will result in smaller, positive twisting (for sheets with non-zero initial curvature). Looking at the even- and odd-crease patterns separately, the fewer creases there are, the greater the twisting. Spacing between creases is also important in prescribing the amount of bending and twisting generated from pinching. When the spacing increases, so does the magnitude of bending and twisting. Sheet stiffness had a small effect on the amount of bending and twisting generated from pinching, where more flexible sheets experience larger deformations.

In this letter, we have identified the potential of shape-morphing by pinching origami, and future research would enhance the capabilities of these programmable systems. For example, we know that origami that is folded about non-uniformly spaced creases can generate twisting without any pinching. Understanding the impact that non-uniformly spaced creases has in conjunction with pinching could result in more varied shape morphing. Additionally, future research could explore the behavior due to pinching origami at different and multiple points along the length of the crease. With greater investigation of the range of motion of pinched origami, future research could develop an inverse design scheme where origami can morph into target shapes using careful crease pattern

design and placement of local actuation(s). Finally, curved-crease sheets have been shown to have unique and programmable stiffness characteristics, so exploring stiffness tuning in conjunction with pinched shape morphing could open up new potential capabilities.

Acknowledgments

The authors would like to thank the Office of Naval Research for their financial support (Grants No. N00014-18-1-2015 # 12461330 and N00014-20-5-B001 # 13209604). The first author would also like to thank the National Science Foundation for their financial support through the Graduate Research Fellowship Program (Grant No. DGE 1841052).

CRediT author statement

Steven R. Woodruff: Conceptualization, Methodology, Software, Formal analysis, Investigation, Writing – Original draft, Writing – Review and editing, Visualization. **Evgueni T. Filipov:** Conceptualization, Methodology, Resources, Writing – Review and editing, Supervision, Project administration, Funding acquisition.

References

[1] Abdelmohsen, S., Adriaenssens, S., Gabriele, S., Olivieri, L., and El-Dabaa, R. (2019). Hygroscapes: Innovative shape shifting façades. In Bianconi, F. and Filippucci, M., editors, *Digital Wood Design: Innovative Techniques of Representation in Architectural Design*, Lecture Notes in Civil Engineering, pages 675–702. Springer International Publishing. https://doi.org/10.1007/978-3-030-03676-8_26.

[2] Agarwal, T., Yun Hann, S., Chiesa, I., Cui, H., Celikkin, N., Micalizzi, S., Barbetta, A., Costantini, M., Esworthy, T., Grace Zhang, L., Maria, C. D., and Kumar Maiti, T. (2021). 4D printing in biomedical applications: emerging trends and technologies. *Journal of Materials Chemistry B*, 9(37):7608–7632. https://doi.org/10.1039/D1TB01335A.

[3] Anumodh, R., Singh, B., and Zuber, M. (2021). Morphing applications in automobiles: a review. *International Journal of Vehicle Design*, 85(1):1–31.

[4] Asfaw, A. M. and Ozbulut, O. E. (2021). Characterization of shape memory alloy energy dissipators for earthquake-resilient structures. *Structural Control and Health Monitoring*, 28(4):e2697. https://doi.org/10.1002/stc.2697.

[5] Badger, J. C., Nelson, T. G., Lang, R. J., Halverson, D. M., and Howell, L. L. (2019). Normalized coordinate equations and an energy method for predicting natural curved-fold configurations. *Journal of Applied Mechanics*, 86(7). https://doi.org/10.1115/1.4043285.

[6] Bende, N. P., Evans, A. A., Innes-Gold, S., Marin, L. A., Cohen, I., Hayward, R. C., and Santangelo, C. D. (2015). Geometrically controlled snapping transitions in shells with curved creases. *Proceedings of the National Academy of Sciences*, 112(36):11175–11180. https://doi.org/10.1073/pnas.1509228112.

[7] Concilio, A. and Ameduri, S. (2020). Morphing wings review: aims, challenges, and current open issues of a technology. *Proceedings of the Institution of Mechanical Engineers, Part C: Journal of Mechanical Engineering Science*. https://doi.org/10.1177/0954406220944423.

[8] Demaine, E. D., Demaine, M. L., Huffman, D. A., Koschitz, D., and Tachi, T. (2014). Characterization of curved creases and rulings: design and analysis of lens tessellations. In Miura, K., Kawasaki, T., Tachi, T., Uehara, R., Lang, R., and Wang-Iverson, P., editors, *Origami 6: Proceedings of the 6th International Meeting on Origami in Science, Mathematics and Education*, volume 1, pages 209–230. American Mathematical Society, Tokyo, Japan. https://doi.org/10.1090/mbk/095.1/20.

[9] Demaine, E. D., Demaine, M. L., Koschitz, D., and Tachi, T. (2015). A review on curved creases in art, design and mathematics. *Symmetry: Culture and Science*, 26(2):145–161. https://doi.org/10.26830/symmetry_2015_2.

[10] Dias, M. A. and Santangelo, C. D. (2012). The shape and mechanics of curved fold origami structures. *Europhysics Letters*, 100(5):54005. https://doi.org/10.1209/0295-5075/100/54005.

[11] Ding, F. and Kareem, A. (2020). Tall buildings with dynamic facade under winds. *Engineering*, 6(12):1443–1453. https://doi.org/10.1016/j.eng.2020.07.020.

[12] Duncan, J. P. and Duncan, J. L. (1982). Folded developables. *Proceedings of the Royal Society of London. Series A, Mathematical and Physical Sciences*, 383(1784):191–205. https://doi.org/10.1098/rspa.1982.0126.

[13] Filipov, E. T., Liu, K., Tachi, T., Schenk, M., and Paulino, G. H. (2017). Bar and hinge models for scalable analysis of origami. *International Journal of Solids and Structures*, 124:26–45. https://doi.org/10.1016/j.ijsolstr.2017.05.028.

[14] Fiorito, F., Sauchelli, M., Arroyo, D., Pesenti, M., Imperadori, M., Masera, G., and Ranzi, G. (2016). Shape morphing solar shadings: A review. *Renewable and Sustainable Energy Reviews*, 55:863–884. https://doi.org/10.1016/j.rser.2015.10.086.

[15] Fuchs, D. and Tabachnikov, S. (1999). More on Paperfolding. *The American Mathematical Monthly*, 106(1):27–35. https://doi.org/10.1080/00029890.1999.12005003.

[16] Gu, H., Shaw, A. D., Amoozgar, M., Zhang, J., Wang, C., and Friswell, M. I. (2020). Twist morphing of a composite rotor blade using a novel metamaterial. *Composite Structures*, 254:112855. https://doi.org/10.1016/j.compstruct.2020.112855.

[17] Holmes, D. P., Roché, M., Sinha, T., and Stone, H. A. (2011). Bending and twisting of soft materials by non-homogenous swelling. *Soft Matter*, 7(11):5188–5193. https://doi.org/10.1039/C0SM01492C.

[18] Hu, W., Lum, G. Z., Mastrangeli, M., and Sitti, M. (2018). Small-scale soft-bodied robot with multimodal locomotion. *Nature*, 554(7690):81–85. https://doi.org/10.1038/nature25443.

[19] Kim, M.-H., Nam, S., Oh, M., Lee, H.-J., Jang, B., and Hyun, S. (2021). Bioinspired, shape-morphing scale battery for untethered soft robots. *Soft Robotics*. https://doi.org/10.1089/soro.2020.0175.

[20] Kim, W., Byun, J., Kim, J.-K., Choi, W.-Y., Jakobsen, K., Jakobsen, J., Lee, D.-Y., and Cho, K.-J. (2019). Bioinspired dual-morphing stretchable origami. *Science Robotics*, 4(36):eaay3493. https://doi.org/10.1126/scirobotics.aay3493.

[21] Kirillova, A. and Ionov, L. (2019). Shape-changing polymers for biomedical applications. *Journal of Materials Chemistry B*, 7(10):1597–1624. https://doi.org/10.1039/C8TB02579G.

[22] Kreyszig, E. (1991). *Differential Geometry*. Dover, New York.

[23] Lang, R. J., Nelson, T. G., Magleby, S. P., and Howell, L. L. (2017). Kinematics and discretization of curved-fold mechanisms. In *Proceedings of the ASME 2017*, Cleveland, OH. ASME. https://doi.org/10.1115/DETC2017-67439.

[24] Liu, K., Hacker, F., and Daraio, C. (2021). Robotic surfaces with reversible, spatiotemporal control for shape morphing and object manipulation. *Science Robotics*, 6(53):eabf5116. https://doi.org/10.1126/scirobotics.abf5116.

[25] Liu, K., Novelino, L. S., Gardoni, P., and Paulino, G. H. (2020). Big influence of small random imperfections in origami-based metamaterials. *Proceedings of the Royal Society A: Mathematical, Physical and Engineering Sciences*, 476(2241):20200236. https://doi.org/10.1098/rspa.2020.0236.

[26] Liu, K. and Paulino, G. H. (2017). Nonlinear mechanics of non-rigid origami: an efficient computational approach. *Proceedings of the Royal Society A: Mathematical, Physical and Engineering Sciences*, 473(2206):20170348. https://doi.org/10.1098/rspa.2017.0348.

[27] Mintchev, S., Shintake, J., and Floreano, D. (2018). Bioinspired dual-stiffness origami. *Science Robotics*, 3(20):eaau0275. https://doi.org/10.1126/scirobotics.aau0275.

[28] Pini, V., Ruz, J. J., Kosaka, P. M., Malvar, O., Calleja, M., and Tamayo, J. (2016). How two-dimensional bending can extraordinarily stiffen thin sheets. *Scientific Reports*, 6: Article 29627. https://doi.org/10.1038/srep29627.

[29] Ricci, A., Ponzio, C., Fabbri, K., Gaspari, J., and Naboni, E. (2021). Development of a self-sufficient dynamic façade within the context of climate change. *Architectural Science Review*, 64(1-2):87–97. https://doi.org/10.1080/00038628.2020.1713042.

[30] Rivera-Tarazona, L. K., Bhat, V. D., Kim, H., Campbell, Z. T., and Ware, T. H. (2020). Shape-morphing living composites. *Science Advances*, 6(3):eaax8582. https://doi.org/10.1126/sciadv.aax8582.

[31] Sakovsky, M. and Ermanni, P. (2020). A thin-shell shape adaptable composite metamaterial. *Composite Structures*, 246:112390. https://doi.org/10.1016/j.compstruct.2020.112390.

[32] Schenk, M. and Guest, S. D. (2011). Origami folding: a structural engineering approach. In Wang-Iverson, P., Lang, R. J., and Yim, M., editors, *Origami 5: Fifth International Meeting of Origami Science, Mathematics, and Education*, pages 291–303. A K Peters/CRC Press, New York, 1st edition. https://doi.org/10.1201/b10971.

[33] Shah, D., Yang, B., Kriegman, S., Levin, M., Bongard, J., and Kramer-Bottiglio, R. (2021). Shape changing robots: Bioinspiration, simulation, and physical realization. *Advanced Materials*, 33(19):2002882. https://doi.org/10.1002/adma.202002882.

[34] Wang, W., Li, C., Cho, M., and Ahn, S.-H. (2018). Soft tendril-inspired grippers: Shape morphing of programmable polymer-paper bilayer composites. *ACS Applied Materials & Interfaces*, 10(12):10419–10427. https://doi.org/10.1021/acsami.7b18079.

[35] Watanabe, Y. and Mitani, J. (2018). Interactive modelling of curved folds with multiple creases considering folding motions. *Computer-Aided Design and Applications*, 16(3):452–465. https://doi.org/10.14733/cadaps.2019.452-465.

[36] Wenz, F., Schmidt, I., Leichner, A., Lichti, T., Baumann, S., Andrae, H., and Eberl, C. (2021). Designing shape morphing behavior through local programming of mechanical metamaterials. *Advanced Materials*, 33(37):2008617. https://doi.org/10.1002/adma.202008617.

[37] Woodruff, S. R. and Filipov, E. T. (2020). A bar and hinge model formulation for structural analysis of curved-crease origami. *International Journal of Solids and Structures*, 204-205:114–127. https://doi.org/10.1016/j.ijsolstr.2020.08.010.

[38] Woodruff, S. R. and Filipov, E. T. (2021). Curved creases redistribute global bending stiffness in corrugations: theory and experimentation. *Meccanica*, 56(6):1613–1634. https://doi.org/10.1007/s11012-020-01200-7.

[39] Wriggers, P. (2008). *Nonlinear finite element methods*. Springer. https://doi.org/10.1007/978-3-540-71001-1.

[40] Yang, Y., Vella, K., and Holmes, D. P. (2021). Grasping with kirigami shells. *Science Robotics*, 6(54):eabd6426. https://doi.org/10.1126/scirobotics.abd6426.

[41] Zhai, Z., Wang, Y., Lin, K., Wu, L., and Jiang, H. (2020). In situ stiffness manipulation using elegant curved origami. *Science Advances*, 6(47):eabe2000. https://doi.org/10.1126/sciadv.abe2000.